Neuroscience Informatics 2 (2022) 100092

Contents lists available at ScienceDirect

Neuroscience Informatics

www.elsevier.com/locate/neuri

Original article

The hemodynamic model solving algorithm by using fMRI measurements

Md. Roni Islam, Sheikh Md. Rabiul Islam *

Department of Electronics and Communication Engineering, Khulna University of Engineering and Technology, Khulna-9203, Bangladesh

ARTICLE INFO

Article history:
Received 2 May 2022
Received in revised form 23 June 2022
Accepted 23 June 2022

Dataset link: https://www.fil.ion.ucl.ac.uk/spm/data/attention/

Dataset link: https://www.fil.ion.ucl.ac.uk/spm/data/face_rep/

Keywords:
Hemodynamic model
Functional magnetic resonance imaging
Biophysical parameters
Hidden states
Cubature Kalman filtering

ABSTRACT

Background and objective: The hemodynamic model is a fundamental approach for successfully monitoring and possibly forecasting brain activities in the biomedical engineering field. The hemodynamic model describes the inner scenario of a blood flowing voxel in a human brain and it is most popular hypothesis on the brain related research activities. The hemodynamic model has nonlinearities in nature. The solution of such type hemodynamic model is researchable work.
Method: There are many model solving algorithms by using fMRI images; recently, Haifeng Wu presented Confounds Square-root Cubature Kalman Filtering and Confounds Square-root Cubature Smoothing (CSCKF-CSCKS) is the latest approach for solving hemodynamic models. The relative accuracy of this model was shown 84%. In this article, in order to achieve better accuracy, the data analysis and model algorithms are presented differently and find new result that was not mentioned earlier.
Result: The data analysis of this experiment shows that if the maximum number of iterations increases three times, the overall accuracy for solving the hemodynamic model raises by 5.76% under the exact type of fMRI measurements used in both cases. We also represent a formula for calculating a relative error to evaluate the performance of these estimations.
Conclusion: A recommendation is made for solving the hemodynamic model algorithm by using fMRI images to get better performance for estimating the model's biophysical parameters and hidden states. As a result, we will find out more accurate scenario of a specific region of human brain by using fMRI images of that region.

1. Introduction

Functional Magnetic Resonance Imaging (fMRI) has demonstrated to be an excellent noninvasive electronic machine for giving three-dimensional images of the brain at per unit of time, allowing physicians to identify active brain regions since its beginnings 1990s [1]. The basic principle of fMRI measures the brain activity by detecting associated changes in blood flow and produces three-dimensional images of the brain. By using these three-dimensional images, we are able to produce real Blood Oxygenation Level Dependent (BOLD) signal. This BOLD signal is described the proper scenario of our brain activity. This BOLD signal is different form in case of different subjects and different brain regions [2,3]. The artificial BOLD signal is also created by using two gamma probability density functions for applying in various simulation purposes [4]. There are several models to describe the inner scenario of brain activation and among them the Buxton hemodynamic model, 1998, is an important one. The Buxton hemodynamic model describes accurately the changes in blood flow and blood oxygenation for successfully monitoring and possibly forecasting brain activity [5–7]. Basically, the hemodynamic model is nonlinear in nature [8,9]. The solution of hemodynamic model is a researchable work. So far as we know, in 2000, J. K. Friston has been taken an important initiative to solve the Buxton hemodynamic model by using Volterra kernel type expansion. Later in 2002, he was used the Bayesian framework to characterize hemodynamic responses [10]. The use of Bayesian framework is help to avoid the Volterra kernel type expansion. In 2004, first time used the local linearization (LL) filter into the fully stochastic hemodynamic model to observe the neuronal activity by J. Riera [11,12]. Finally, in 2008, J. K. Friston was able to make an algorithm for solving hemodynamic

* Corresponding author.
E-mail addresses: roniislam73@gmail.com (Md.R. Islam), robi@ece.kuet.ac.bd (S.Md.R. Islam).

https://doi.org/10.1016/j.neuri.2022.100092

Table 1
Description of dataset.

S/N	Dataset name	Source	Functional images	Structural images	Remarks
01	Attention to motion	[19]	360 pcs	1 pcs	Realigning, slice-timing corrected, normalizing and properly smoothing
02	Face Rep	[21]	351 pcs	1 pcs	Raw-EPI (Echo-planner Imaging)

model named Dynamic Expectation Maximization (DEM) which was a routine method of inverting hemodynamic model [13]. But, the DEM have two major problems, one, it cannot able to perform in low frequency interference factors; two, it cannot able to measure hidden states, biophysical parameters more accurately. In order to get more accuracy, Martin Havlicek, in 2011, proposed an estimation scheme that based on cubature Kalman filtering (CKF) framework [14,15]. This algorithm first performs the square root cubature Kalman filtering (SCKF) for forward pass and then uses square root cubature Rauch-Tung-Striebel (RST) smoother (SCKS) for backward pass [16]. The accuracy of SCKF-SCKS approach is better than DEM to estimate hidden states, biophysical parameters of hemodynamic model. But, the performance in low frequency interference factors is not still possible by the SCKF-SCKS approach. To overcome this problem, in 2018, Mingzhi Lu proposed a new algorithm based on the previous SCKF-SCKS approach and able to solve the hemodynamic model by using fMRI images under low frequency interference factors [17,18]. For this reason, Mingzhi Lu proposed a low frequency interference (confound) factors considered algorithm which is now called confound SCKF-confound SCKS (CSCKF-CSCKS) algorithm. Mingzhi Lu has been updated the CSCKF-CSCKS in 2020 which algorithm shows that when the signal to interference ratio (SNR) is less than 21 dB, the estimated error reduced to 16%, whereas the traditional algorithm reduces it to only 73% [18]. As a result, the accuracy of CSCKF-CSCKS approach under low frequency interference factors is 84%. But, the improvement of accuracy is a continuous process. In this paper, we will able to show that the accuracy of CSCKF-CSCKS approach achieves 89.76% if we increase the maximum numbers of iterations three times from its present value. We also prove in this paper how this achievement is possible with explanations.

2. Materials and methods

Generally speaking, we break down our methodology into four steps. We used a multi-subject dataset in the first step to properly validate our improved algorithm. We scanned fMRI images from multiple subjects using a 3tesla fMRI scanner. The image acquisition related experimental designs and all parameter settings of these acquisition processes are broadly and detailed described in articles [19] and [21]. Second step, we utilized image processing software SPM that is integrated with MATLAB to extract statistical data in required format that represented the existence of blood activation and metabolic function in the brain. The SPM software produces a real time series shown in Fig. 2 according to the instructions described in the chapter 35 named 'Dynamic Causal Modeling for fMRI' on the SPM12 on the SPM12 manual [20]. Third step, by using the forward filtering algorithm process named CSCKF; we are reduced BOLD response of that time series. Fourth step, we used inverse process named CSCKS to determine biophysical parameters and hidden states of the hemodynamic model.

2.1. Datasets

For our good understanding, we recall the attention dataset as a first subject and the face dataset as second subject in Table 1. Before reducing time series, the face rep data must be realigning, slice-timing corrected, normalizing and properly smoothing by the instruction described in the chapter 31 named 'Face fMRI data' on the SPM12 manual [20].

In the Fig. 1, the 3D normalized view of structural images of first subject and second subjects are shown with their resolution.

The complete hemodynamic model relating input synaptic activity u(t) to BOLD signal y(t) is described by the sets of characteristic equations listed in articles [5–7]. These equations can be described as specific form which is also described in Minghzu Lu article [17,18]. The CSCKF-CSCKS algorithm has two parts, which are described sequentially below.

2.2. Forward filtering passes (CSCKF)

The algorithm related equations are presented here

$$\hat{x}_0^a = E\left[x_0^a\right] = \left[\hat{x}_0^T, 0, 0, 0, 0\right]^T = \left[x_0, \theta_0, \beta_{0|h}, \beta_{0|m}, \beta_{0|l}, 0_p, 0_s, 0_v, 0_m\right]^T \tag{1}$$

$$S_0^a = \mathrm{chol}\left(E\left[\left(x_0^a - \hat{x}_0^a\right)\left(x_0^a - \hat{x}_0^a\right)^T\right]\right) = \mathrm{diag}(S_0, S_p, S_s, S_v, S_m) \tag{2}$$

$$\chi^a_{I,t-1|t-1} = S^a_{t-1|t-1}\xi_t + \hat{\chi}^a_{t-1|t-1} \tag{3}$$

$$\chi^{x,u,\theta}_{I,t|t-1} = F\left(\chi^{a(x)}_{I,t-1|t-1}, \chi^{a(u)}_{I,t-1|t-1}, \chi^{a(\theta)}_{I,t-1|t-1}\right) + \chi^{a(q,y,w)}_{I,t-1|t-1} \tag{4}$$

$$\hat{\chi}_{t|t-1} = \frac{1}{m}\sum_{i=1}^{m}\chi^{x,u,\theta}_{I,t|t-1} \tag{5}$$

$$S_{t|t-1} = qr(X_{t|t-1}) \tag{6}$$

$$X_{t|t-1} = \frac{1}{\sqrt{m}}[\chi^{x,u,\theta}_{1,t|t-1} - \hat{\chi}_{t|t-1}, \chi^{x,u,\theta}_{2,t|t-1} - \hat{\chi}_{t|t-1}, \text{II....}, \chi^{x,u,\theta}_{m,t|t-1} - \hat{\chi}_{t|t-1}] \tag{7}$$

$$Y_{I,t|t-1} = g(\chi^x_{I,t|t-1}, \chi^u_{I,t|t-1}, \chi^\theta_{I,t|t-1}) + \chi^{al}_{I,t-1|t-1} \tag{8}$$

$$\hat{y}_{t|t-1} = \frac{1}{\sqrt{m}}\sum_{i=1}^{m}Y_{I,t|t-1} \tag{9}$$

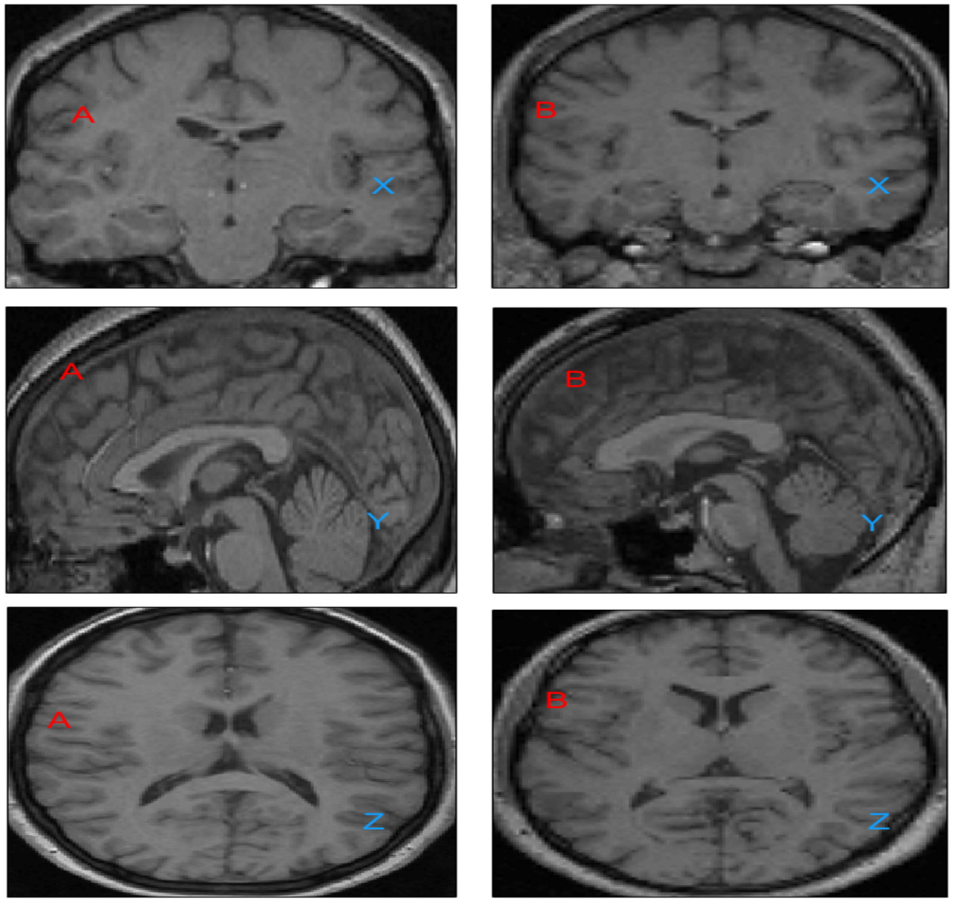

Fig. 1. Input structural images (X, Y, and Z coordination) of first subject (marked by A) from attention dataset and Second subject (marked by B) from face dataset with resolutions $157 \times 189 \times 68$ and $79 \times 95 \times 79$, respectively.

$$S_{yy,t|t-1} = qr(Y_{t|t-1}) \tag{10}$$

$$Y_{t|t-1} = \frac{1}{\sqrt{m}}[Y_{1,t|t-1} - \hat{y}_{t|t-1}, Y_{2,t|t-1} - \hat{y}_{t|t-1}, \ldots\ldots\ldots\ldots\ldots Y_{m,t|t-1} - \hat{y}_{t|t-1}] \tag{11}$$

$$P_{xy,t|t-1} = X_{t|t-1}Y^{T}_{t|t-1} \tag{12}$$

$$K_t = (P_{xy,t|t-1}/S^{T}_{xy,t|t-1})/S_{xy,t|t-1} \tag{13}$$

$$\hat{\chi}_{t|t} = \hat{\chi}_{t|t-1} + K_t(y_t - \hat{y}_{t|t-1}) \tag{14}$$

$$S_{t|t} = qr([X_{t|t-1} - K_tY_{t|t-1}]) \tag{15}$$

The whole processes was executed in MATLAB until the last fMRI image was used.

2.3. Backward smoothing filter (CSCKS)

$$\hat{x}^{a}_{t|t} = \left[\hat{x}^{T}_{t|T}, 0, 0, 0, 0\right]^{T} \tag{16}$$

$$S^{a}_{t|t} = \text{diag}(S_{t|T}, S_{q,T}, S_v, S_{w,T}, S_r) \tag{17}$$

$$\chi^{a}_{I,t|t} = S^{a}_{t|t}\xi_i + \hat{\chi}^{a}_{t|t} \tag{18}$$

$$\chi^{x,u,\theta}_{I,t+1|t} = F\left(\chi^{a(x)}_{I,t|t}, \chi^{a(u)}_{I,t|t}, \chi^{a(\theta)}_{I,t|t}\right) + \chi^{a(q,y,w)}_{I,t|t} \tag{19}$$

$$\hat{\chi}_{t+1|t} = \frac{1}{m}\sum_{i=1}^{m}\chi^{x,u,\theta}_{I,t+1|t} \tag{20}$$

$$S_{t+1|t} = qr(X_{t+1|t}) \tag{21}$$

$$X_{t+1|t} = \frac{1}{\sqrt{m}}[\chi^{x,u,\theta}_{1,t+1|t} - \hat{\chi}_{t|t-1}, \chi^{x,u,\theta}_{2,t+1|t} - \hat{\chi}_{t|t-1}, \text{ II....}, \chi^{x,u,\theta}_{m,t|t-1} - \hat{\chi}_{t|t-1}] \tag{22}$$

$$P_{x'x,t+1|t} = X'_{t|t}X^{T}_{t+1|t} \tag{23}$$

Table 2
Parameters and initial conditions settings of CSCKF-CSCKS algorithm.

Parameters	Initial conditions
State vector	$x_{0\|0} = [0, 0, 0, 0]$
Model parameters	$\theta = [\theta_1, \theta_2, \theta_3, \theta_4]$
Noise matrix	$\beta_{0\|0} = [0, 0, 0, 0, 0, 0]$
Noise matrix	$\beta = [2.4,\ -0.4,\ 1.0,\ -0.8,\ 0.6,\ 0.2]/0.5$
Error covariance matrix	$Q_{x\|0} = \text{diag}[10^{-2}, 10^{-2}, 10^{-2}, 10^{-2}]$
Error covariance matrix	$Q_{\beta\|0} = \text{diag}[10^{-3}, 10^{-3}, 10^{-3}, 10^{-3}, 10^{-3}, 10^{-3}]$
Error covariance matrix	$Q_{\theta\|0} = \text{diag}[10^{-20}, 10^{-20}, 10^{-20}, 10^{-20}]$
Covariance Matrix	$Q_p = \text{diag}[10^{-6}, 10^{-6}, 10^{-6}, 10^{-6}]$
Covariance Matrix	$Q_s = \text{diag}[10^{-4}, 10^{-4}, 10^{-3}]$
Covariance Matrix	$Q_v = \text{diag}[10^{-4}, 10^{-4}, 10^{-4}, 10^{-4}, 10^{-4}, 10^{-4}]$
Covariance Matrix	$Q_m = \text{diag}[10^{-3}]$
Integration step	$\Delta t = 0.2$ s

$$X'_{t|t} = \frac{1}{\sqrt{m}}[\chi_{1,t|t}^{a(x,u,\theta)} - \hat{\chi}_{t|t}^{a(x,u,\theta)}, \chi_{2,t|t}^{a(x,u,\theta)} - \hat{\chi}_{t|t}^{a(x,u,\theta)},\ II...., \chi_{m,t|t}^{a(x,u,\theta)} - \hat{\chi}_{t|t}^{a(x,u,\theta)}] \tag{24}$$

$$A_t = (\frac{P_{x'x,t+1|t}}{S_{t+1|t}^T})/S_{t+1|t} \tag{25}$$

$$\hat{\chi}_{t|T}^{s} = \hat{\chi}_{t|t}^{a(x,u,\theta)} + A_t(\hat{\chi}_{t+1|T}^{s} - \hat{\chi}_{t+1|t}) \tag{26}$$

$$S_{t|T}^{s} = qr([X'_{t|t} - A_t X_{t+1|t}, A_t S_{t+1|T}^{s}]) \tag{27}$$

So, the estimation processes are sequentially executing in MATLAB coding until find out model parameters and hidden states.

2.4. Measurement of log likelihood and relative error

The predicted error is calculated by the following formula, which allows us to calculate maximum log likelihood of the model data that met the stopping condition of iteration process.

$$e_t = y_t - \hat{y}_t \tag{28}$$

$$\log p(y_{1:T} \mid \theta) = -\frac{T}{2}\log(2\pi) - \frac{T}{2}\sum_{t=1}^{T}[\log \mid S_{yy,t|t-1}S_{yy,t|t-1}^{T} \mid + \frac{e_t e_t^T}{S_{yy,t|t-1}S_{yy,t|t-1}^{T}}] \tag{29}$$

For comparison between two same types of data, we use the relative error formula to compare one concerning the second one. The following formula defines the relative error-

$$e_t = \left[\sum_{l=1}^{k}\sum_{p=1}^{r}|D_{lp} - d_{lp}| \Big/ \sum_{l=1}^{k}\sum_{p=1}^{r}|d_{lp}|\right] \times 100\% \tag{30}$$

Where, capital D and small d represent the compared data one with respect to the second one, respectively.

3. Result and discussion

With the help of CSCKF-CSCKS algorithm, the estimated biophysical parameters and hidden states are measured in two different cases; case I, the number of maximum iterations are set 20, and the case II, the number of maximum iterations are set 64. The parameters and initial conditions settings of CSCKF-CSCKS approach are described in Table 2.

The image processing work of this experiment have been done in SPM (SPM12 version,https://www.fil.ion.ucl.ac.uk/spm/software/) software. The algorithm's scripts, result analysis related all tasks have been performed in MATLAB R2020b (MATLAB 9.9 version) software. The time series of both subjects are different to each other, but the comparative results of various parameters (biophysical parameters, hidden states, and maximum log-likelihood) are remained same in case of first subject and second subject. For this reason, it has concluded that the proposed algorithm is work properly in single and multi-subject in both cases. These changes are adjusted in MATLAB coding by using the necessary debugging process.

The constructed time series is demonstrated in the Fig. 2 on V5 region of first and second subject. This figure shows the amplitude with respect to time.

In both cases (I & II), we compare the results with the true values which were collected from the prestigious journals. The well-known and universal acceptable true values of the hemodynamic biophysical parameters are 0.65, 0.41, 0.98, 0.32, 0.34, 0.02, and 0.5 represent the rate of signal decay, rate of flow dependent elimination, hemodynamic transit time, resting oxygen extraction fraction, Grubb's exponent, region specific ratios of the echo, neuronal efficacy, respectively [21]. By using the time series and the CSCKF algorithm, we are able to extract BOLD response which is demonstrated in the following Fig. 3.

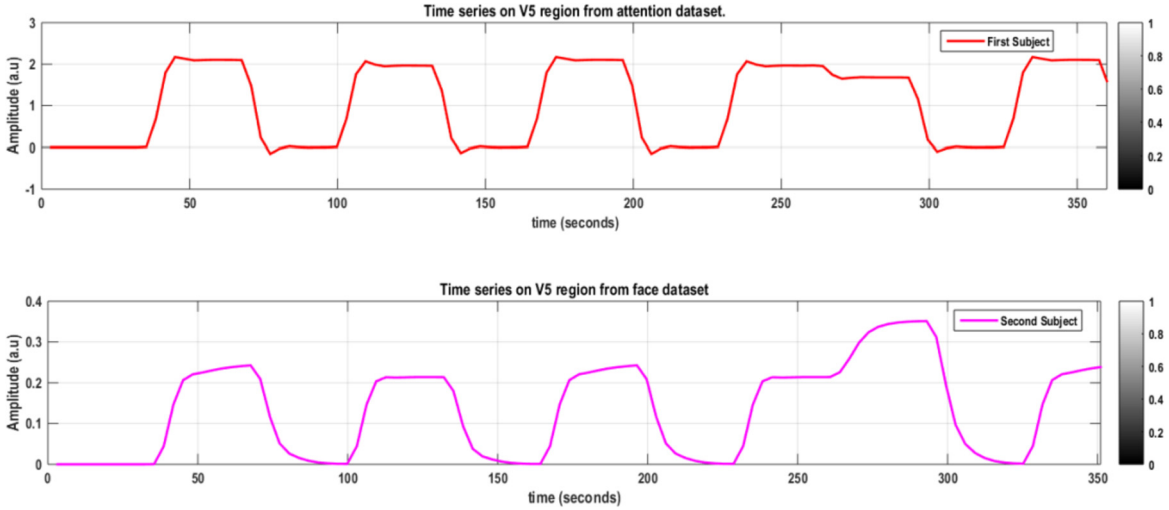

Fig. 2. Time series on V5 region of first subject (colored by red) from attention dataset and second subject (colored by magenta) from face dataset. The attention and face dataset contains 360 and 351 functional fMRI volumetric images and these time series are produced from them by using SPM software.

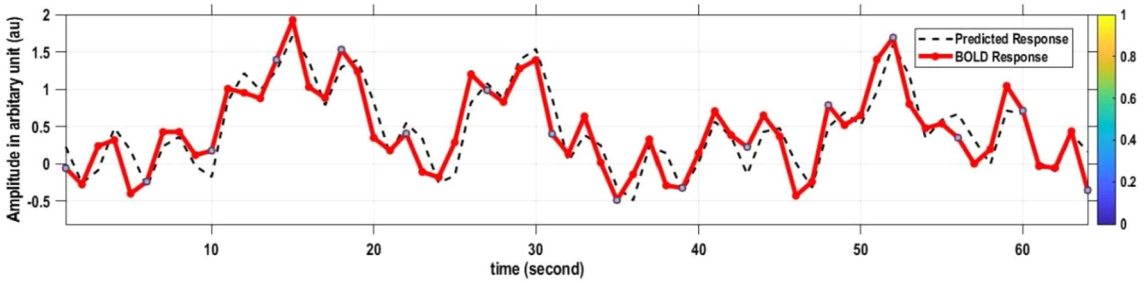

Fig. 3. BOLD Response curve.

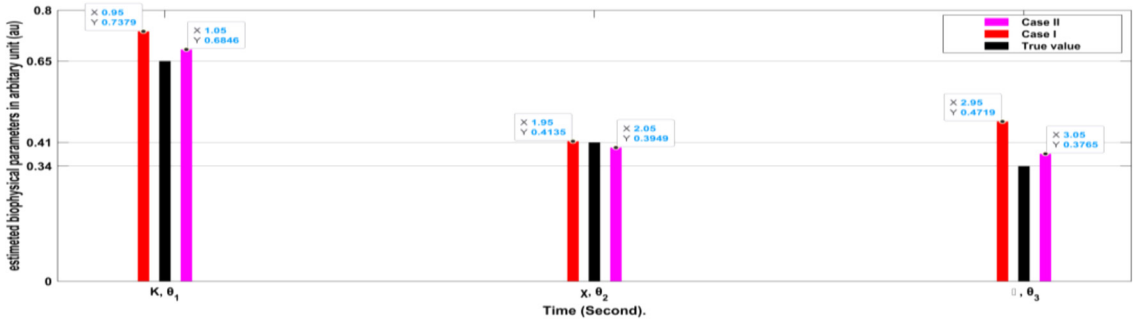

Fig. 4. The simulation result of biophysical parameters in cases of I, II with true value, Case I maximum numbers of iterations are 20 (red marked curve, legend 'old'). Case II maximum numbers of iterations are 64 (magenta marked curve, legend 'new').

3.1. Comparison of biophysical parameters

In Fig. 4 shows the estimated results of biophysical parameters. The first biophysical parameter 'rate of signal decay' is 0.6846, 0.7379, and 0.65 in case of I, II, and true value, respectively. The estimated rate of signal decay is 94.68%, 86.48% closed to true value in case II, I, respectively. So, the parameters extraction accuracy of case II is 8.2% better than case I. At the same point of view, the second biophysical parameter 'the rate of flow dependent elimination' is almost same in case I, II with true value. The third biophysical parameter 'Grubb's exponent' is 89.23%, 61.21% closed to true value in case II, I, respectively. So, the accuracy of case II is 28.02% more than case I.

3.2. Comparison of hidden states

Fig. 5 shows the estimated results of hidden states. The estimated curves at time point 7, 23, 32.5, 37.5, 46, 55 and 63 are coincided to each other and rest of time the estimated curves are deviated from each other maintained a numerical relationship. The compressed patterns of 7, 23 time points are much more consisted than that of 32.5, 37. On the other hands, the deviation lengths of 8-22, 24-32 time points are much more looped than that of 33-36, 38-45.

These observations state that at the first two mentioned time points, the relevant slices area of the human brain are busy to a specified task and after that, the relevant slices of the human brain take rest to attend next actions. The deviations of estimated curves (blue, red, and yellow colored) from case II are much more consisted with the deviations of the estimated curves (black colored) from true values

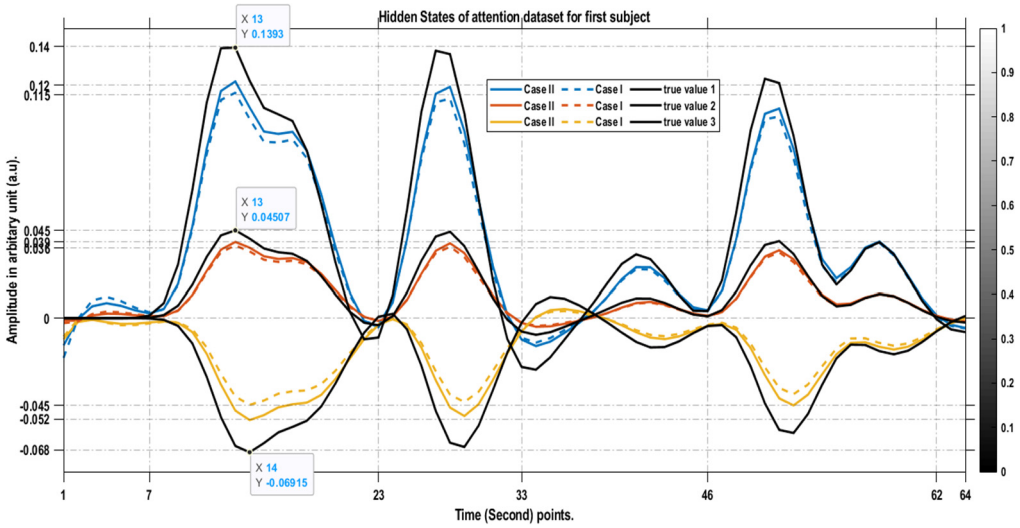

Fig. 5. The simulation results of hidden states in case of I, II with true value. Case I maximum numbers of iterations are 20 (legend 'Case I'). Case II maximum numbers of iterations are 64 (legend 'Case II').

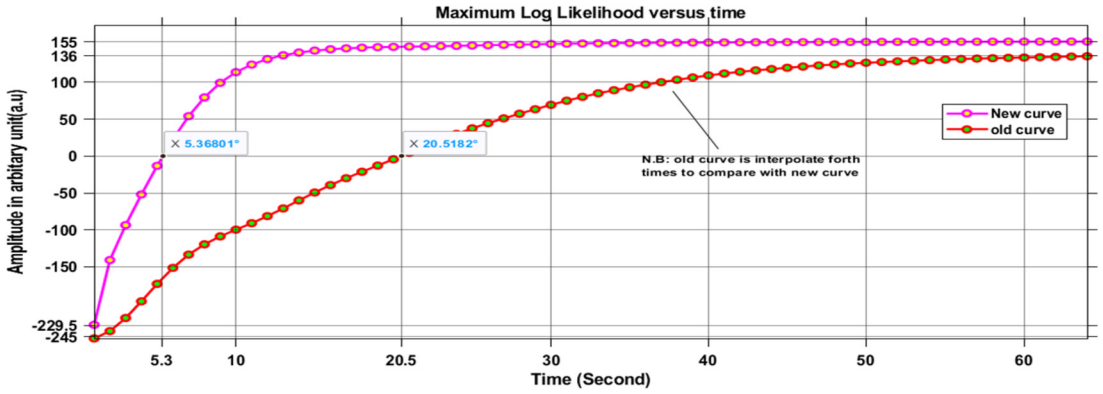

Fig. 6. Maximum log likelihood curve versus time.

than that of case I (dotted blue, red, and yellow colored). The deviation of 8-22 time points are [0.1393-(-0.06915)] 0.20845au (arbitary unit) for true value, 0.172au for case II (82.51% similarity with true value),and 0.16au for case I (76.75% similarity with true value). The case II algorithm is to estimate hidden states 5.76% more accurate than that of case I algorithms. So, it is clear from the Fig. 5 that if the maximum numbers of iterations increase three times, the accuracy of case II algorithm is more accurate to determine hidden states than that of other algorithms.

3.3. Comparison of log likelihood

Fig. 6 shows the estimated maximum log likelihood versus time. For comparing with new maximum log likelihood curve, we interpolate the old curve data forth times.

If we carefully observed the Fig. 6, it shows that the deviation of new curve is more than that of old curve. For the old curve, the actual X value will be as (20.5182*64/80/4) 4.10364°, on the other hand, the actual X value of new curve is 5.36801°. The measured deviation of the new curve is 23.47° (5.36801-4.10364/5.35801) more than the old curve. So, if the maximum numbers of iterations increase three times, the maximum log likelihood curve is more deviation than previous position. Iterate until the stopping condition is met. We evaluate log likelihood of each iteration and terminate the optimization when the increase of the negative log likelihood is less than a tolerance value e.g. 10^{-3} [16]. If we again carefully observe the Fig. 6, we find out that the old curve reach negative to zero log likelihood almost forth times slower than that of new curve. From negative to zero log likelihood, the old curve need 20.5 second, on the other hand, the new curve need 5.3 second. So, if we increase the maximum number of iterations three times, the log likelihood fourth times faster than that of old case. As a result, at least 15.2 second before, the log likelihood of the 64 iterations system overcomes negative values than that of 20 iterations system. So, the 64 iterations system get more times for reaching the stopping condition. For this reason, the accuracy of 64 iterations system is more than 20 iterations system.

3.4. Relative error (%) calculation for hidden states

Fig. 7 shows the relative error curve of two data calculated using the equation (43) mentioned in the methodology section. Curve 1 represents the error estimation between the CSCKS algorithm, which used the maximum number of iterations equal to 5, concerning the CSCKS algorithm, which used the maximum number of iterations equal to 20. Curve 2 represents the error estimation between the CSCKS

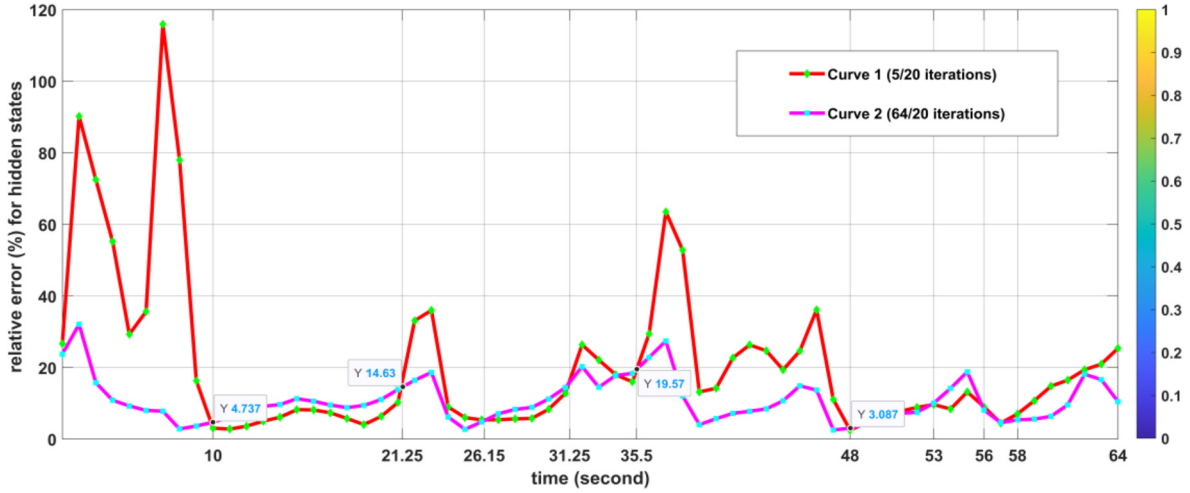

Fig. 7. Relative error (%) calculation for hidden states.

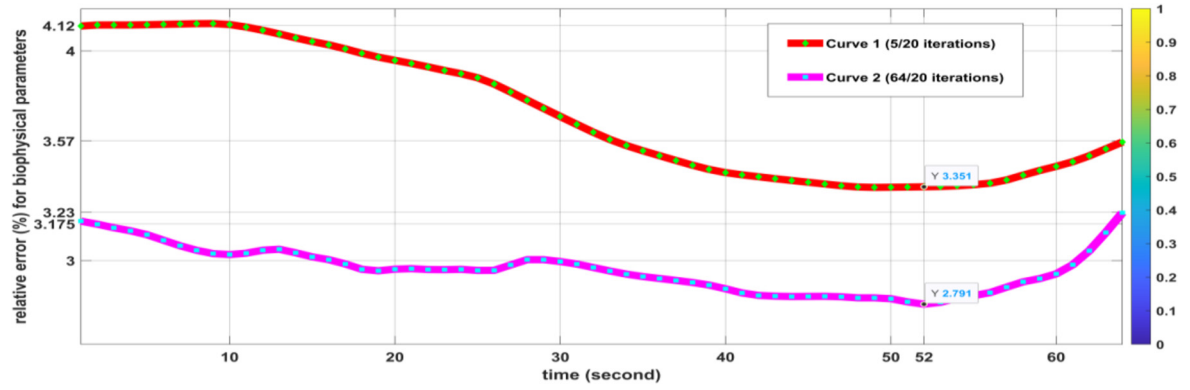

Fig. 8. Relative error (%) calculation for biophysical parameters.

algorithm, which used a maximum number of iterations equal to 64, with respect to the CSCKS algorithm, which used the maximum number of iterations equal to 20. In Fig. 7, we calculated and plotted the error estimation in the case of hidden state data. If we carefully observe the figure, we can see that in the time point 0-10, the relative error of curve 1 much more deviates from curve 2. The change of error of curve 1 is 4% to 116%, while the change of error of curve 2 is 4% to 32%. That means the similarity between the curve II is 27.58% (32/116) better than that of curve I. So, if the maximum number of iterations increases three times in this period, relatively less error occurs in the hidden states estimation process.

But in time point 10, the two error curves intersect each other's, which means in this time, the error is almost the same in the two cases. For the same explanation, the time point 10-21.25 seconds, the relatively more error occurs in the hidden states estimation process if the number of maximum iterations increases due to the opposite position of curve 2 than curve 1. So, suppose we more carefully observed the whole graph. In that case, we can conclude that the relatively less error always occurs if the number of maximum iterations increases except at the time point 10-21.25 (11.25 second), 26.15-31.25 (5.1 seconds), and 53-56 (3 seconds). As a result, the relatively less error occurs at 44.65 out of 64 seconds. The experiment results recommend that if the number of maximum iterations increases three times, a relatively 31% less error occurs in the hidden states estimation process.

3.5. Relative error (%) calculation for biophysical parameters

Fig. 8 shows the comparative result of the curve as mentioned above 1 and curve 2 for the biophysical parameters. The relative error of curve 1 for the biophysical parameters is reduced from 4.12% to 3.57%. On the other hand, the relative error of curve 2 increases from 3.175% to 3.23%. But, in the overall conclusion, the relative error of curve 2 is always less than that of curve 1. The change of error of curve 1 is a minimum 3.351% to 4.12%. On the other hand, the change of error of curve 2 is a minimum 2.791% to 3.23%.

4. Conclusion

The recently introduced CSCKF-CSCKS approach can simulate all frequency interference factors, i.e., low, medium, and high confounds. It can make hidden states, model biophysical parameters, and BOLD response more accurately than existing methods. The biophysical parameters, the hidden conditions, and maximum log-likelihood estimated results show that if the maximum number of iterations increases three times, error optimization gets more times. Due to this reason, the maximum log-likelihood met the stopping condition more than faster. As a result, minimum 5.76%, 8.2% to 28.02%, and 23.47% accuracy occur in hidden states, biophysical parameters, and maximum log-likelihood estimation. So, it is recommended for the user of the CSCKF-CSCKS algorithm to set the maximum number of iterations

three times of present value to get better performance and accuracy for estimating hidden states of the hemodynamic model. As a result, we strongly recommend that the maximum number of iterations be set at 64 instead of 20 at the CSCKF-CSCKS algorithm for better performance.

Human and animal rights

The authors declare that the work described has not involved experimentation on humans or animals.

Funding

This work did not receive any grant from funding agencies in the public, commercial, or not-for-profit sectors.

Author contributions

All authors attest that they meet the current International Committee of Medical Journal Editors (ICMJE) criteria for Authorship.

Declaration of competing interest

The authors declare that they have no known competing financial or personal relationships that could be viewed as influencing the work reported in this paper.

Data availability statement

The data was acquired raw images related zip file is available in an open access SPM website. The links of attention and face dataset are (https://www.fil.ion.ucl.ac.uk/spm/data/attention/) and (https://www.fil.ion.ucl.ac.uk/spm/data/face_rep/), respectively.

Acknowledgements

The authors wish to thank department of Electronics and Communication Engineering (ECE) staffs and professors for sporting equipment and other facilities. This work was not supported in part by a grant.

References

[1] Hans H. Schild, MRI: Made Easy, Schering AG Publishing Company, Berlin, Germany, 1990.
[2] G.K. Aguirre, E. Zarahn, M. D'sposito, The variability of human, BOLD hemodynamic responses, NeuroImage 8 (1998) 360–369.
[3] D. Handwerker, J. Ollinger, M. D'espsito, Variation of BOLD hemodynamic response across subjects and brain regions and their effects on statistical analyses, NeuroImage 21 (2004) 1639–1651.
[4] M.R. Islam, Model design of hemodynamic response function within FIR basis for functional magnetic resonance imaging, Int. J. Adv. Eng. Manag. 3 (2021) 719–726.
[5] R.B. Buxton, Lawrence R. Frank, A model for the coupling between cerebral blood flow and oxygen metabolism during neural stimulation, J. Cereb. Blood Flow Metab. 17 (1997) 64–72.
[6] R.B. Buxton, Eric C. Wong, Lawrence R. Frank, Dynamics of blood flow and oxygenation changes during brain activation: the balloon model, Magn. Reson. Med. 39 (1998) 855–864.
[7] R.B. Buxton, Kamil Uludag, David J. Dubowitz, Tomas T. Liu, Modeling the hemodynamic response to brain activation, NeuroImage 23 (2004) s220–s233.
[8] G.S. Berns, A.W. Song, H. Mao, Continuous functional magnetic response imaging reveals dynamic nonlinearities of 'dos-response' curves for finger opposition, J. Neurosci. 19 (1999) 1–6.
[9] A. Mechelli, C. Price, J.K. Friston, Nonlinear coupling between evoked rCBF and BOLD signals: a simulation study of hemodynamic responses, NeuroImage 14 (2001) 862–872.
[10] K.J. Friston, A. Mechelli, R. Turner, C.J. Price, Nonlinear responses in fMRI: the balloon model, Volterra kernels, and other hemodynamics, NeuroImage 12 (2000) 466–477.
[11] J.C. Jimenez, T. Ozaki, Local linearization filters for non-linear continuous-discrete state space models with multiplicative noise, Int. J. Control 76 (2003) 1159–1170.
[12] J. Riera, J. Watanable, I. Kazuki, M. Naoki, E. Aubert, T. Ozaki, R. Kawashima, A state space model of the hemodynamic approach: nonlinear filtering of BOLD signals, NeuroImage 21 (2004) 547–567.
[13] K.J. Friston, N. Trujillo Barreto, J. Daunizeau, DEM: a variational treatment of dynamic systems, NeuroImage 41 (2008) 849–885.
[14] I. Arasaratnam, S. Haykin, Cubature Kalman filters, IEEE Trans. Autom. Control 54 (06) (2009, June) 1254–1269.
[15] I. Arasaratnam, S. Haykin, T.R. Hurd, Cubature Kalman filtering for continuous discrete systems: theory and simulations, IEEE Trans. Signal Process. 58 (10) (2010, October) 4977–4993.
[16] Martin Havilicek, Karl J. Friston, Jiri Jan, Vince D Brazdil, Milan Calhoun, Dynamic modeling of neuronal responses in fMRI using cubature Kalman filtering, NeuroImage 56 (2011) 2109–2128.
[17] M. Lu, H. Wu, Y. Zeng, A new algorithm for solving hemodynamic models in fMRI under low frequency interference, Proc. Comput. Sci. 131 (2018) 485–494.
[18] Haifeng Wu, Mingzhi Lu, Yu Zeng, State estimation of hemodynamic model for fMRI under confounds: SSM method, IEEE J. Biomed. Health Inform. 24 (3) (March 2020).
[19] C. Buchel, K.J. Friston, Modulation of connectivity in visual pathways by attention: cortical interactions evaluated with structural equation modeling and fMRI, Cereb. Cortex 7 (1997) 768–778.
[20] SPM12 Manual, the manual prepared by the functional imaging laboratory methods group and honorary members, Wellcome Centre for Human Neuroimaging, London, UK, 2020, the manual download link: https://www.fil.ion.ucl.ac.uk/spm/doc/manual.pdf.
[21] R.N.A. Hanson, T. Shallice, M.L. Gorno Tempini, R.J. Dolan, Face repetition in implicit and explicit memory tests as measured by fMRI, Cereb. Cortex 12 (2002) 178–186.